Journal of Biomolecular NMR, **11:** 387–405, 1998.
KLUWER/ESCOM

Sequential resonance assignment of medium-sized $^{15}N/^{13}C$-labeled proteins with projected 4D triple resonance NMR experiments

Thomas Szyperski*, Bogdan Banecki**, Daniel Braun & Ralf W. Glaser***
Institut für Molekularbiologie und Biophysik, Eidgenössische Technische Hochschule-Hönggerberg, CH-8093 Zürich, Switzerland

Received 12 September 1997; Accepted 27 November 1997

Key words: automated resonance assignment; NMR assignments; reduced-dimensionality triple-resonance experiments; resolution enhancement in NMR.

Abstract

We recently introduced a new line of reduced-dimensionality experiments making constructive use of axial peak magnetization, which has so far been suppressed as an undesirable artifact in multidimensional NMR spectra [Szyperski, T., Braun, D., Banecki, B. and Wüthrich, K. (1996) *J. Am. Chem. Soc.*, **118**, 8146–8147]. The peaks arising from the axial magnetization are located at the center of the doublets resulting from projection. Here we describe the use of such projected four-dimensional (4D) triple resonance experiments for the efficient sequential resonance assignment of $^{15}N/^{13}C$-labeled proteins. A 3D $\underline{H}^{\alpha/\beta}$ $\underline{C}^{\alpha/\beta}$(CO)NHN experiment is recorded either in conjunction with 3D HNN<$\underline{CO}$,$\underline{CA}$> or with the newly presented 3D HNN$\underline{CAHA}$ scheme. The first combination yields sequential assignments based on the measurement of $^{13}C^{\alpha}$ chemical shifts and provides a complete ^{1}H, ^{13}C and ^{15}N resonance assignment of polypeptide backbone and CH_n^{β} moieties. When employing the second combination, $^{13}C{=}O$ chemical shifts are not measured, but the sequential assignment relies on both $^{13}C^{\alpha}$ and $^{1}H^{\alpha}$ chemical shifts. The assignment is performed in a semi-automatic fashion using the program XEASY in conjunction with the newly implemented program SPSCAN. This program package offers routines for the facile mutual interconversion of single-quantum and zero/double-quantum frequencies detected in conventional and reduced-dimensionality spectra, respectively. In particular, SPSCAN comprises a peak picking routine tailored to cope with the distinct peak patterns of projected NMR experiments performed with simultaneous acquisition of central peaks. Data were acquired at 13 °C for the N-terminal 63-residue polypeptide fragment of the 434 repressor. Analysis of these spectra, which are representative for proteins of about 15 kDa when working at commonly used temperatures around 30 °C, demonstrates the efficiency of our approach for the assignment of medium-sized $^{15}N/^{13}C$ doubly labeled proteins.

Introduction

The use of triple-resonance experiments for the resonance assignment of polypeptide chains *via* heteronuclear scalar connectivities (Montelione and Wagner, 1989a, b; Ikura et al., 1990; Kay et al., 1990a; for a review see: Edison et al., 1994) is nowadays a standard approach which neatly complements the assignment protocol based on ^{1}H–^{1}H nuclear Overhauser effects (NOE) (Wüthrich, 1986). Although the structure of a small or medium-sized protein ($\leq$ 15 kDa) may often be solved with ^{1}H NMR spectroscopy alone, its isotope labeling becomes mandatory when (i) the structural study is hampered by poor ^{1}H chemical shift dispersion, e.g. in purely α-helical (Wishart et al., 1991) or partly unfolded proteins (Neri et al., 1992a), (ii) the structural refinement shall include heteronuclear scalar coupling constants (Eberstadt et al., 1995), (iii) the hydration of the protein shall

* To whom correspondence should be addressed. ** Present address: Department of Molecular and Cellular Biology, University of Gdansk, Kladki 24, 80-822 Gdansk, Poland. ***Present address: Institut für Molekularbiologie, Universität Jena, D-07708 Jena, Germany.

be investigated using 3D ^{15}N- and/or ^{13}C-resolved [^{1}H,^{1}H]-NOESY/ROESY (Otting et al., 1991; Qian et al., 1993), (iv) the dynamics of the protein shall be elucidated by measurement of heteronuclear spin relaxation parameters (Nirmala and Wagner, 1988; Kay et al., 1989; Peng and Wagner, 1992; Szyperski et al., 1993a; Yamazaki et al., 1994a), or (v) the protein shall be studied as a part of a macromolecular complex, e.g. using isotope filtered spectroscopy (Otting and Wüthrich, 1990). Moreover, triple resonance NMR spectra are highly amenable to a fast automated analysis (Friedrichs et al., 1994; Zimmerman et al., 1994; Morelle et al., 1995; Bartels et al., 1996; Buchler et al., 1997; Lukin et al., 1997) yielding the $^{13}C^{\alpha/\beta}$ chemical shifts at an early stage of the assignment procedure. This enables both the identification of regular secondary structure elements without reference to NOEs (Spera and Bax, 1991) and the derivation of (ϕ,ψ)-angle constraints which serve to reduce the number of cycles consisting of NOESY peak assignment and structure calculation (Luginbühl et al., 1995). Hence, NMR experiments tailored for the efficient assignment of small and medium-sized ^{15}N/^{13}C doubly labeled proteins meet with a wide interest.

The use of 3D HNNCA/3D HNN(CO)CA offers the most sensitive approach to derive sequential resonance assignments *via* scalar connectivities (Cavanagh et al., 1996). However, except for smaller proteins it is quite generally limited by $^{13}C^{\alpha}$ chemical shift degeneracy. To resolve the assignment ambiguities, at least one of the three nuclei attached to the α-carbon – namely H^{α}, C' or C^{β} – has to be additionally invoked to establish sequential connectivities (Table 1). Recording of either 3D HNNCACB/3D CBCA(CO)NHN or 4D HNNCAHA/4D HACA(CO)NHN is attractive, because the large number of NMR experiments usually employed for the structure determination of ^{15}N/^{13}C-labeled proteins is not further increased. However, when recording 4D spectra one has to accept short maximal evolution times in at least two of the dimensions, which results in a relatively large uncertainty in the chemical shift measurements.

We have introduced a projection technique for reducing the dimensionality of triple resonance experiments (Szyperski et al., 1993b,c). In these experiments (Brutscher et al., 1994, 1995a,b; Szyperski et al., 1994a, 1995, 1996, 1997; Löhr and Rüterjans, 1995; Rexroth et al., 1995; Simorre et al., 1995; Bracken et al., 1997; Pellecchia et al., 1998) the chemical shifts of the projected dimension give rise to a cosine-modulation of the transfer amplitude, yielding peak doublets encoding n chemical shifts in a n–1 dimensional spectrum. Most important, the joint incrementation of two chemical shift evolution times allows to record projected 4D experiments with maximal evolution times being typical for conventional 3D experiments (Szyperski et al., 1993b,c, 1994a,b, 1995, 1996; Brutscher et al., 1995; Bracken et al., 1997; Fernández et al., 1997; Pellecchia et al., 1998). Furthermore, we have very recently demonstrated (Szyperski et al., 1996) that axial coherences can be observed as peaks located at the center of the doublets. These central peaks enable both, the unambiguous assignment of multiple doublets with degenerate chemical shifts in the other dimensions and the symmetrization of the spectrum (Baumann et al., 1981; Brutscher et al., 1995a,b; Szyperski et al., 1995, 1996). Hence, observation of central peaks not only restores the dispersion of the parent, higher-dimensional experiment, but also provides access to the reservoir of axial peak magnetization (Szyperski et al., 1996). Here we demonstrate that such projected 4D triple resonance experiments offer efficient routes for the sequential assignment of medium-sized ^{15}N/^{13}C-labeled proteins.

Methods

The 3D HNN<CO,CA> experiment

The 3D HNN<CO,CA> experiment (Szyperski et al., 1995) correlates the backbone chemical shifts $\Omega(^{1}H_{i}^{N})$, $\Omega(^{15}N_{i})$, $\Omega(^{13}C{=}O_{i-1})$ and $\Omega(^{13}C_{i}^{\alpha})$ of residue i via $^{1}J\{^{15}N_{i}, {}^{13}C_{i}^{\alpha}\}$ and $^{1}J\{^{15}N_{i}, {}^{13}C{=}O_{i-1}\}$. Simultaneously, $^{2}J\{^{15}N_{i}, {}^{13}C_{i-1}^{\alpha}\}$ yields sequential correlations including $\Omega(^{1}H_{i}^{N})$, $\Omega(^{15}N_{i})$, $\Omega(^{13}C{=}O_{i-1})$ and $\Omega(^{13}C_{i-1}^{\alpha})$. The underlined letters denote that ^{13}C=O and $^{13}C^{\alpha}$ are jointly observed, and the brackets indicate that the experiment is performed in a 'bifurcated' out-and-back fashion (Szyperski et al., 1996). Since $^{1}J\{^{15}N_{i}, {}^{13}C{=}O_{i-1}\} > J\{^{15}N_{i}, {}^{13}C_{i}^{\alpha}\}$, ^{13}C=O has to be detected in quadrature to observe central peaks located at $\Omega(^{13}C{=}O)$, and $\Omega(^{13}C^{\alpha})$ gives rise to the doublets (Figure 1A). Note that we had denoted this experiment 3D COHNNCA according to the covalent structure of the CO-HN-C^{α} moiety, but subsequently renamed it according to its bifurcated magnetization transfer (Szyperski et al., 1996).

Table 1. Approaches to resolve ^{13}C chemical shift degeneracy with triple resonance NMR spectroscopy

(A) Combination of	3D HNNCA[a]	and	3D HNN(CO)CA[b]	with
either	3D HNN(CA)HA[c]	and	3D HNN(COCA)HA[d]	
or	3D HNNCO[a]	and	3D HNN(CA)CO[e]	
or	3D HNN(CA)CB[f]	and	3D HNN(COCA)CB[g]	
(B) Increase of the dimensionality				
	4D HNNCAHA[h]	and	4D HACA(CO)NHN[h]	
(C) Introduction of a carbon–carbon magnetization transfer step				
	3D HNNCACB[i]	and	3D CBCA(CO)NHN[j]	
(D) Employment of the reduced-dimensionality approach				
	3D HNNCAHA	and	3D $\underline{H}^{\alpha/\beta}\underline{C}^{\alpha/\beta}$(CO)NHN[k]	

[a] Kay et al. (1990a).
[b] Bax and Ikura (1991).
[c] Clubb et al. (1992a).
[d] Clubb and Wagner (1992).
[e] Clubb et al. (1992b), Matsuo et al. (1996).
[f] Yamazaki et al. (1994b).
[g] Shan et al. (1996).
[h] Boucher et al. (1992); Kay et al. (1992); Olejniczak et al. (1992).
[i] Wittekind and Müller (1993).
[j] Grzesiek and Bax (1992b).
[k] Szyperski et al. (1994a).

The new implementation of the 3D $\underline{H}^{\alpha/\beta}$ $\underline{C}^{\alpha/\beta}$ (CO)NHN experiment

The 3D $\underline{H}^{\alpha/\beta}$ $\underline{C}^{\alpha/\beta}$(CO)NHN experiment combines two approaches to increase the information content of a 3D triple resonance spectrum (Table 1), i.e., projection and homonuclear ^{13}C-^{13}C magnetization transfer (Szyperski et al., 1994a), and thus correlates up to seven chemical shifts: $\Omega(^1H^{\beta1}_{i-1})$, $\Omega(^1H^{\beta2}_{i-1})$, $\Omega(^{13}C^{\beta}_{i-1})$, $\Omega(^1H^{\alpha}_{i-1})$ and $\Omega(^{13}C^{\alpha}_{i-1})$ of residue i–1 with $\Omega(^1H^{N}_{i})$ and $\Omega(^{15}N_i)$ of residue i. The underlined letters indicate that $\Omega(^1H^{\alpha/\beta})$ and $\Omega(^{13}C^{\alpha/\beta})$ are observed in a common dimension. In order to exploit steady-state $^{13}C^{\alpha/\beta}$ magnetization for the observation of central peaks, ^{13}C has to be detected in quadrature and $\Omega(^1H^{\alpha/\beta})$ is encoded in an in-phase splitting (Szyperski et al., 1996). This enables the use of steady-state $^{13}C^{\alpha/\beta}$ magnetization being discarded by axial peak suppression in the parent 4D experiment, which has been used for fractionally deuterated proteins (Nietlispach et al., 1996). Our approach (Figure 1B) yields the subspectra I and II containing either doublets or central peaks, respectively (Szyperski et al., 1996). This allows for their unambiguous distinction and prevents from their mutual overlap, and the central peaks are quite generally observed when the doublets are recorded with a workable signal-to-noise ratio (Szyperski et al., 1996). Subspectrum II provides the information of 3D CBCA(CO)NHN even if the resonances of the aliphatic protons are severely broadened. The addition of the subspectra for obtaining absorptive central peaks and doublets in a single spectrum is also not beneficial in view of the resulting decrease of the signal-to-noise ratio by $\sqrt{2}$: the subspectra are out of phase by 90° so that their noise is statistically not correlated when both are phased absorptive (Cavanagh and Rance, 1990). Compared with the previous one (Szyperski et al., 1994a), the new scheme uses (i) a semi constant-time module (Grzesiek and Bax, 1993a) for ^1H-frequency labeling, (ii) shaped pulses on $^{13}C^{\alpha/\beta}$ and $^{13}C{=}O$, (iii) a sensitivity enhancement scheme (Palmer et al., 1991), and (iv) pulsed field gradients for coherence pathway rejection (Bax and Pochapsky, 1992; Wider and Wüthrich, 1993) allowing for a minimal four-step phase cycle. No gradients were introduced into the constant-time delay for $^{13}C^{\alpha/\beta}$ chemical shift evolution to fully exploit it for frequency labeling. A detailed description of the new implementation is available from the authors.

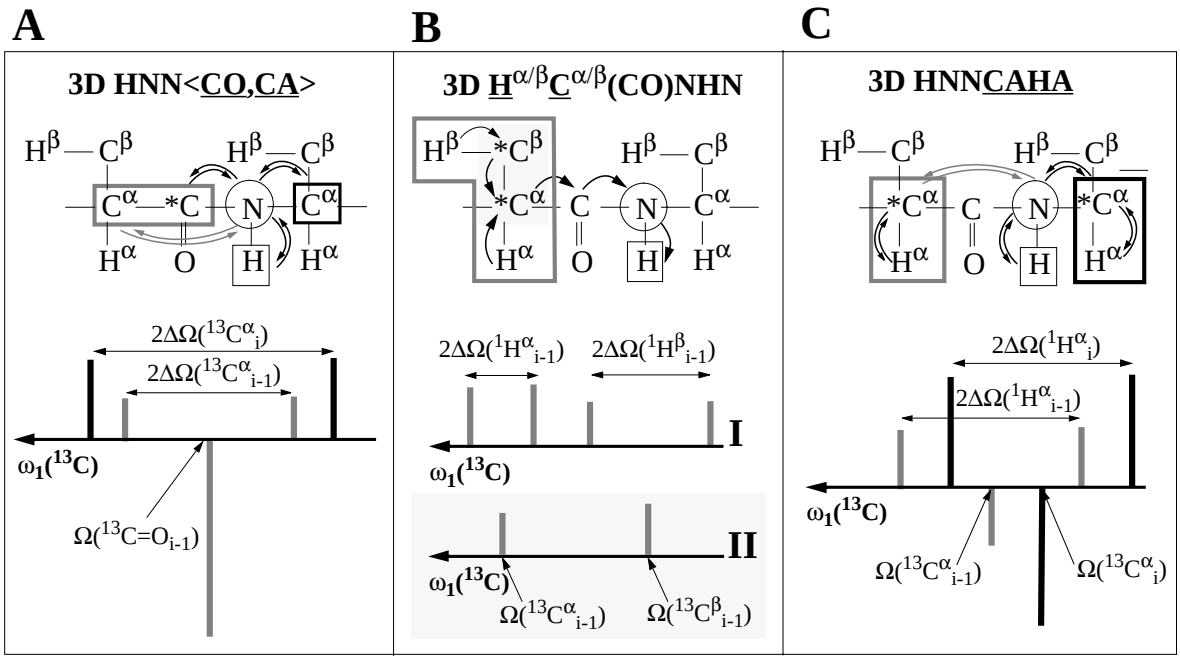

Figure 1. Magnetization transfer pathways (top) and stick diagrams of the peak pattern observed along $\omega_1(^{13}C)$ (bottom) for (A) 3D HNN<CO,CA>, (B) 3D $H^{\alpha/\beta}C^{\alpha/\beta}$(CO)NHN and (C) 3D HNNCAHA. The boxes comprise nuclei whose chemical shifts are measured in the common dimension ω_1, and the nuclei which are detected in quadrature in t_1 are marked with an asterisk. Bold solid and hatched boxes indicate intraresidual and sequential connectivities, respectively, and the resulting signals sketched in the stick diagrams are represented accordingly. In (B), the $^{13}C^{\alpha/\beta}$ nuclei whose steady-state magnetization is used to detect central peaks, as well as the resulting subspectrum II, are highlighted in grey. The magnetization is frequency labeled with $\Omega(^{15}N_i)$ (encircled nucleus) during t_2 and detected on $\Omega(^1H_i^N)$ (boxed nucleus) during t_3. HSQC-type transfers based on one-bond and two-bond couplings are represented by black and grey arrows, respectively. In (A), the in-phase splittings $2\Delta\Omega(^{13}C^\alpha)$ are equal to $2\kappa \cdot \delta\Omega(^{13}C^\alpha)$, where κ and $\delta\Omega(^{13}C^\alpha)$ are the scaling factor applied for $^{13}C^\alpha$ chemical shift evolution and the chemical shift difference with respect to the apparent $^{13}C^\alpha$ carrier position, respectively. In (B) and (C), the in-phase splittings $2\Delta\Omega(^1H^\alpha)$ are equal to $2\kappa \cdot \delta\Omega(^1H)[\gamma(^1H)/\gamma(^{13}C)]$, where κ, $\delta\Omega(^1H)$ and $\gamma(X)$ denote the scaling factor applied for ^1H chemical shift evolution, the chemical shift difference with respect to the apparent ^1H carrier position, and the gyromagnetic ratio of nucleus X, respectively.

The new 3D HNNCAHA experiment

The 3D HNNCAHA experiment correlates $\Omega(^1H_i^N)$, $\Omega(^{15}N_i)$, $\Omega(^{13}C_i^\alpha)$ and $\Omega(^1H_i^\alpha)$ of residue i via $^1J\{^{15}N_i, ^{13}C_i^\alpha\}$. A simultaneous transfer via $^2J\{^{15}N_i, ^{13}C_{i-1}^\alpha\}$ yields sequential correlations between $\Omega(^1H_i^N)$, $\Omega(^{15}N_i)$, and $\Omega(^{13}C^\alpha_{i-1})$ and $\Omega(^1H^\alpha_{i-1})$. The underlined letters indicate that $\Omega(^{13}C^\alpha)$ and $\Omega(^1H^\alpha)$ are measured in a common dimension (Szyperski et al., 1993b). Following Boucher et al. (1992a,b), we chose an 'out-and-back' version to minimize the time during which transverse $^{13}C^\alpha$ magnetization is present (Figure 2). The magnetization transfer from $^{13}C^\alpha$ to $^1H^\alpha$ is performed in an HSQC-manner to reduce the loss from passive $^1J\{^{13}C^\alpha, ^{13}C^\beta\}$ couplings during $^1H^\alpha$ chemical shift evolution. This allows for an upscaling of the $^1H^\alpha$ relative to the $^{13}C^\alpha$ chemical shift evolution times (Szyperski et al., 1993b, 1994). The evolution of $\Omega(^{13}C^\alpha)$ is implemented in a semi constant-time fashion to minimize losses from $^1J\{^{13}C^\alpha, ^{13}C^\beta\}$ and $T_2(^{13}C^\alpha)$-relaxation. In order to observe doublets and centers, $^{13}C^\alpha$ has to be detected in quadrature (Szyperski et al., 1996) and $\Omega(^1H^\alpha)$ is encoded in the in-phase splitting (Figure 1C). For studies at pH > 6, the sensitivity of the 3D HNNCAHA experiment could be further improved for rapidly exchanging amide protons by the implementation of a water flip-back approach (Grzesiek and Bax, 1993b).

Following product-operator descriptions (Sørensen et al., 1983) of published 4D HNNCAHA schemes (Boucher et al., 1992b; Kay et al., 1992; Olejniczak et al., 1992) and considering that $\sin(\pi^1J_{NH}\tau_1) \cong \sin(\pi^1J_{NH}\tau_2)$, the transfer functions of 3D HNNCAHA are given by (Figure 2):

$$
\begin{aligned}
&[^1H^N \rightarrow {}^1H^\alpha] : \sin^4(\pi^1J_{NH}\tau_2)\sin^2(\pi^1J_{NA}\tau_3)\\
&\times \cos^2(\pi^2J_{NA}\tau_3)\cos[\Omega(^{15}N_i)t_2]\sin^2(\pi^1J_{CH}\tau_4)\\
&\times \cos(\pi^{\mathbf{1}}\mathbf{J_{CC}}\tau_{\mathbf{4}})\cos[\pi^{\mathbf{1}}\mathbf{J_{CC}}(\tau_{\mathbf{4}}+\lambda\mathbf{t_1})]\\
&\times \cos[\Omega(^{13}C^\alpha_i)t_1]\cos[\kappa\Omega(^1H^\alpha_i)t_1] \qquad (1a)
\end{aligned}
$$

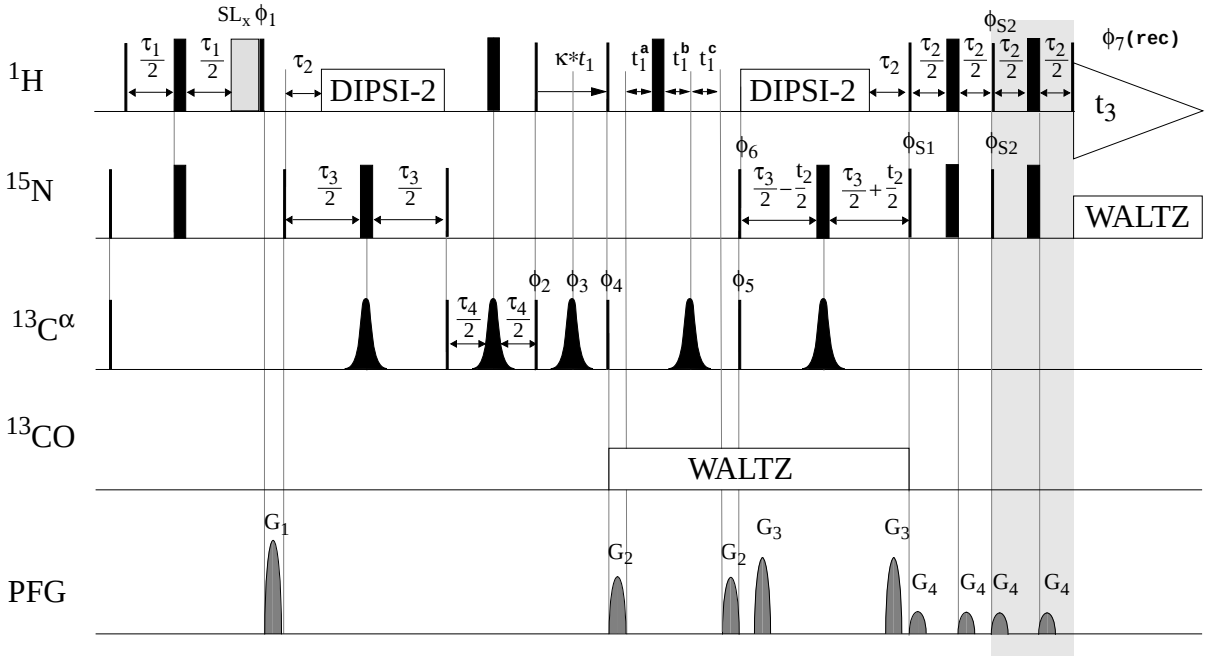

Figure 2. Experimental scheme for the 3D HNNCAHA experiment. Rectangular 90° and 180° pulses are indicated by thin and thick vertical bars, respectively, and phases are indicated above the pulses. Where no radio-frequency phase is marked, the pulse is applied along x. The scaling factor κ for ^{1}H chemical shift evolution is set to 1.70. The 90° pulse lengths were: 11 μs for ^{1}H and $^{13}C^\alpha$, and 40 μs for ^{15}N. The 180 °C pulses on $^{13}C^\alpha$ are of Gaussian shape (truncation at 5%) and 120 μs duration, and have been optimized for a ^{1}H resonance frequency of 600 MHz. DIPSI-2 (Shaka et al., 1988) (rf = 3.8 kHz) is employed to decouple ^{1}H during the heteronuclear magnetization transfers, and WALTZ16 (Shaka et al., 1983) is used for decoupling of ^{15}N (rf = 1.6 kHz) and ^{13}CO (rf = 0.7 kHz). The length of the spin-lock purge pulse (Otting and Wüthrich, 1988) SL_x is 2.5 ms. To implement the sensitivity enhancement scheme of Palmer et al. (1991), the pulses and delays in the shaded box are added and t_1 increments are recorded in an interleaved manner, with ϕ_{S1} = x and ϕ_{S2} = y or with $\phi_{S1} = -x$ and ϕ_{S2} = y. The ^{1}H carrier is placed at the position of the solvent line at 4.88 ppm for the first three ^{1}H pulses and the first DIPSI-2 period, then switched to 2.96 ppm during the first delay $\tau_4/2$, and subsequently switched back to 4.88 ppm during t_1^c. The $^{13}C^\alpha$ and ^{15}N carriers are set to 52.7 ppm and 115 ppm, respectively. The duration and strengths of the sine-bell shaped PFGs are: G_1 (3.5 ms, 40 G/cm); G_2 (344 μs, 15 G/cm); G_3 (344 μs, 30 G/cm); G_4 (344 μs, 8 G/cm). The recovery delay after G_1 is set to 500 μs. The delays have the following values: τ_1 = 5.0 ms, τ_2 = 5.5 ms, τ_3 = 28 ms, τ_4 = 2.0 ms. ^{13}C-frequency labeling is achieved in a semi constant-time fashion with $t_1^a(0)$ = 708.5 μs, $t_1^b(0)$ = 51.8 μs, $t_1^c(0)$ = 655.3 μs, Δt_1^a = 62.5 μs, Δt_1^b = 51.7 μs, $\Delta t_1^c = -10.8$ μs. Hence, the fractional increase of the semi constant-time period with t_1 equals $\lambda = 1 + \Delta t_1^c/\Delta t_1^a = 0.83$. Note that the acquisition was started with the second complex point while the first one was obtained by linear prediction (Stephenson, 1988), so that zero first-order phase correction was achieved along ω_1. Phase cycling: $\phi_1 = 2(y), 2(-y)$; ϕ_2 = y; ϕ_3 = x, −x; ϕ_4 = y; ϕ_5 = x; ϕ_6 = x; ϕ_7 (receiver) = 2(x), 2(−x). Quadrature detection in t_1(^{13}C) and t_2(^{15}N) is accomplished by altering the phases ϕ_5 and ϕ_6, respectively, according to States-TPPI (Marion et al., 1989).

$$[^1H^N \rightarrow {}^{13}C^\alpha] : (-1)\sin^4(\pi {}^1J_{NH}\tau_2) \times \sin^2(\pi {}^1J_{NA}\tau_3)\cos^2(\pi {}^2J_{NA}\tau_3)\cos[\Omega({}^{15}N_i)t_2H] \times \cos^{\mathbf{2}}(\pi {}^{\mathbf{1}}J_{CH}\tau_4)\cos[\pi {}^{\mathbf{1}}\mathbf{J_{CC}}(\mathbf{2\tau_4} + (\kappa+\lambda)\mathbf{t_1})] \times \cos[\Omega({}^{13}C^\alpha_i)t_1] \quad (1b)$$

$$[^1H^N \rightarrow {}^1H^\alpha_{i-1}] : \sin^4(\pi {}^1J_{NH}\tau_2)\sin^2(\pi {}^2J_{NA}\tau_3) \times \cos^2(\pi {}^1J_{NA}\tau_3)\cos[\Omega({}^{15}N_i)t_2H]\sin^2(\pi {}^1J_{CH}\tau_4) \times \cos(\pi {}^{\mathbf{1}}\mathbf{J_{CC}}\tau_4)\cos[\pi {}^{\mathbf{1}}\mathbf{J_{CC}}(\tau_4 + \lambda\mathbf{t_1})] \times \cos[\Omega({}^{13}C^\alpha_{i-1})t_1H] \times \cos[\kappa\Omega({}^1H^\alpha_{i-1})t_1] \quad (1c)$$

$$[^1H^N \rightarrow {}^{13}C^\alpha_{i-1}] : (-1)\sin^4(\pi {}^1J_{NH}\tau_2) \times \sin^2(\pi {}^2J_{NA}\tau_3)\cos^2(\pi {}^1J_{NA}\tau_3)\cos[\Omega({}^{15}N_i)t_2H] \times \cos^2(\pi_1 J_{CH}\tau_4)\cos[\pi {}^{\mathbf{1}}\mathbf{J_{CC}}(\mathbf{2\tau_4} + (\kappa+\lambda)\mathbf{t_1})] \cos[\Omega({}^{\mathbf{13}}\mathbf{C^\alpha_{i-1}})\mathbf{t_1}] \quad (1d)$$

where $^1J_{NH}$, $^1J_{NA}$ $^2J_{NA}$, $^1J_{CH}$ and $^1J_{CC}$ denote the scalar couplings between $^1H^N_i$ and $^{15}N_i$, $^{15}N_i$ and $^{13}C^\alpha_i$, $^{15}N_i$ and $^{13}C^\alpha_{i-1}$, $^{13}C^\alpha$ and $^1H^\alpha$, and $^{13}C^\alpha$ and $^{13}C^\beta$, respectively, and Ω(X) represents the chemical shift of nucleus X. κ indicates the scaling factor applied for $^1H^\alpha$ chemical shift evolution and λ denotes the fractional increase of the semi constant-time delay with t_1 (see legend of Figure 2). Since glycyl residues possess a second α-proton instead of a β-carbon, the cosine-terms highlighted in bold have to be substituted by a single term $\cos^2(\pi {}^1J_{CH}\ \tau_4)$ for these residues. Note that glycyls also give rise to doublets of doublets of low intensity. These originate from the cosine

modulation of the transfer amplitude with both $^1H^\alpha$ chemical shifts (see also Equation (6d) in Szyperski et al. (1995) describing the origin of such doublets of doublets in 3D HNN<CO,CA>). Terms (1a) and (1c) lead to peak doublets observed along ω_1 at $\Omega(^{13}C_i^\alpha) \pm \kappa\ \Omega(^1H_i^\alpha)$ and $\Omega(^{13}C_{i-1}^\alpha) \pm \kappa\ \Omega(^1H_{i-1}^\alpha)$, respectively, while terms (1b) and (1d) represent the central peaks at $\Omega(^{13}C_i^\alpha)$ and $\Omega(^{13}C_{i-1}^\alpha)$. Hence, up to six cross peaks are observed for each residue in a 3D HNNCAHA experiment recorded with simultaneous acquisition of central peaks (Figure 1C). Setting $\tau_3 = 28$ ms for the magnetization transfer from ^{15}N to $^{13}C^\alpha$ yields nearly maximal intensity for both the intraresidual and sequential connectivities.

The peak doublets are attenuated by T_2-relaxation with a loss factor equal to

$$\exp\{-2\tau_2/T_2(^1H^N)\}\exp\{-2\tau_3/T_2(^{15}N)\} \times \exp\{-(2\tau_4+\lambda t_1)/T_2(^{13}C^\alpha)\} \times \exp\{-\kappa t_1/T_2(^1H^\alpha)\} \quad (2a)$$

while the corresponding factor for the central peaks is given by

$$\exp\{-2\tau_2/T_2(^1H^N)\}\exp\{-2\tau_3/T_2(^{15}N)\} \times \exp\{-[2\tau_4+(\kappa+\lambda)t_1]/T_2(^{13}C^\alpha)\} \quad (2b)$$

The optimal value for τ_4 depends on the transfer functions (Equation 1) and the relaxation of transverse $^{13}C^\alpha$ magnetization. Figure 3 shows that $\tau_4 = 2.0$ ms ensures comparable peak intensities of doublets and central peaks for both non-glycyl and glycyl residues. For glycyls, the smaller initial amplitude is at least partly compensated by the absence of dephasing due to the passive $^1J_{CC}$ scalar coupling during t_1. If 3D HNNCAHA shall be employed with 3D $H^{\alpha/\beta}C^{\alpha/\beta}$(CO)NHN, it is strongly recommended to use the same values for the κ and the $^1H^\alpha$ carrier position for the two experiments. This allows for a visual comparison of the in-phase splittings.

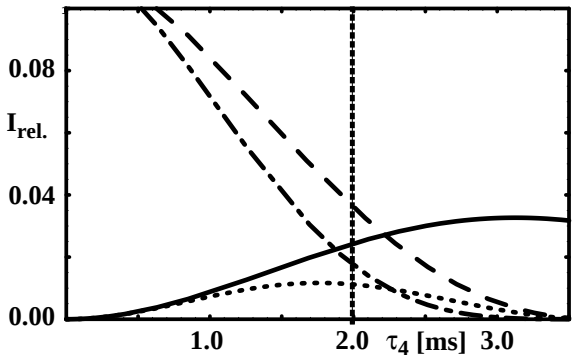

Figure 3. Magnetization transfer in 3D HNNCAHA. Variation with τ_4 of the expressions (1a) (solid line; intraresidual doublets observed for non-glycyl residues) and (1b) (dashed line; intraresidual central peaks of non-glycyl residues), provided that $t_2(^{15}N) = t_1(^{13}C) = t_1(^1H) = 0$ ms, assuming that $^1J_{NH} = 92$ Hz, $^1J_{NA} = 11$ Hz, $^2J_{NA} = 7$ Hz, $^1J_{CH} = 135$ Hz, $^1J_{CC} = 35$Hz, and considering attenuation due to transverse relaxation according to Equation (2a) with $T_2(^{15}N) = T_2(^1H^N) = 50$ ms, $T_2(^{13}C^\alpha) = T_2(^1H^\alpha) = 15$ ms. The curve of (1a) (solid line) has been scaled down to 1/2 to account for the fact that the transfer amplitude yields peak doublets. The dotted and the dashed-and-dotted lines represent the corresponding curves for glycyl residues, and the dotted vertical line indicates the value of $\tau_4 = 2.0$ ms chosen for the current implementation of the experiment.

Computer support for the analysis of projected 4D experiments

Semi-automatic analysis of the NMR spectra was performed using the program XEASY (Bartels et al., 1995) in conjunction with the newly implemented program SPSCAN (R. W. Glaser and K. Wüthrich, to be published). This program package offers routines for the facile mutual interconversion of single-quantum and zero/double-quantum frequencies (Figure 4). In particular, the peak picking routine of SPSCAN has been tailored to cope with the demands of the presently employed spectra. It takes the backbone ^{15}N and $^1H^N$ chemical shifts from 2D [^{15}N, ^1H]-HSQC (Bodenhausen and Ruben, 1980) as initial input. Assuming Gaussian or Lorentzian lineshapes, SPSCAN identifies central peaks and peak doublets by fitting chemical shifts, linewidths and volumes. For the unambiguous identification of the doublets, the program makes use of the distinct peak patterns in the projected 4D spectra (Figure 1). In 3D HNN<CO,CA> and 3D HNNCAHA central peaks are readily identified due to their negative sign, while in 3D $H^{\alpha/\beta}C^{\alpha/\beta}$(CO)NHN they are present only in subspectrum II. [$\omega_1(^{13}C/^1H)$, $\omega_3(^1H^N)$]-strips taken at the backbone ^{15}N chemical shifts are subsequently symmetrized about the position of the central peaks. This increases the signal-to-noise ratio for the doublets (Szyperski et al., 1995) and eliminates other doublets exhibiting very similar or identical ^{15}N and $^1H^N$ chemical shifts, but different centers (Figure 5) (see also Figure 2 in Szyperski et al., 1996). The peak doublets serve to derive 4D peak lists comprising [$\Omega(^{13}C{=}O)$, $\Omega(^{13}C^\alpha)$, $\Omega(^{15}N)$, $\Omega(^1H^N)$] or [$\Omega(^1H^\alpha)$, $\Omega(^{13}C^\alpha)$, $\Omega(^{15}N)$, $\Omega(^1H^N)$]. In 3D HNN<CO,CA> and 3D HNNCAHA, sequential and intraresidual connectivities are putatively distinguished assuming that the latter are more intense. Based on the 4D peak lists, SPSCAN performs a

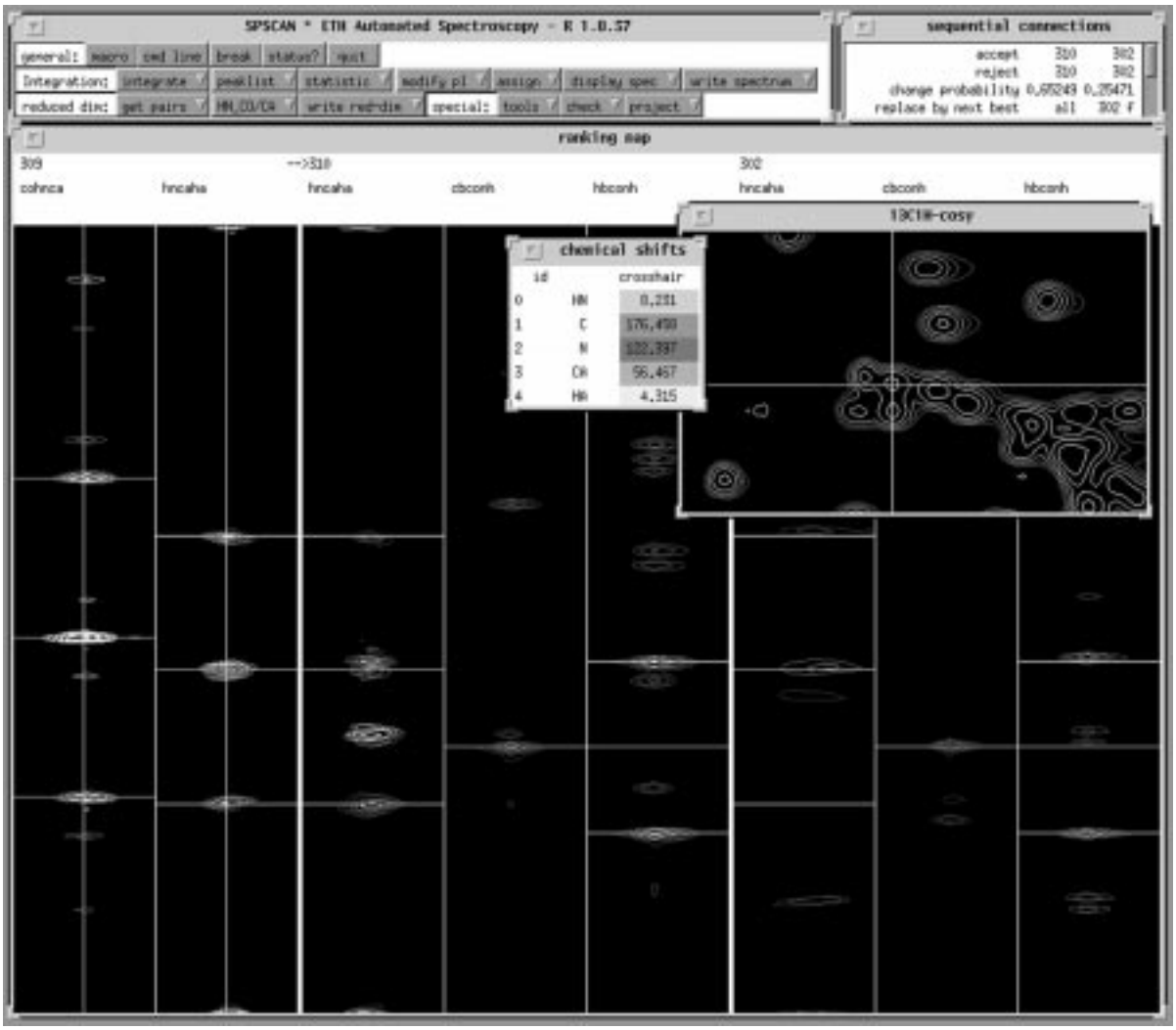

Figure 4. User interface of SPSCAN. The window indicated with 'ranking map' shows [ω_1, ω_3]-strips ranked by SPSCAN that were taken from 3D HNN<CO,CA> ('cohnca'), from 3D HNNCAHA ('hncaha'), and from subspectrum II ('cbconh') and subspectrum I ('hbconh') of 3D $H^{\alpha/\beta}C^{\alpha/\beta}$(CO)NHN. As an example, the two left-most strips exhibit the intraresidual connectivities of spin system 309 (Lys 9). The subsequent strips three to five belong to the sequential neighbour 310 (Arg 10), and strips six to eight belong to spin system 302 (Ile 2). The two spin systems 310 and 302 were ranked first and second in an automatic search using 3D HNNCAHA/3D $H^{\alpha/\beta}C^{\alpha/\beta}$(CO)NHN. The corresponding probabilities derived from the SPSCAN scoring function are given in the window denoted 'sequential connections'. For the facile comparison of single and zero/double quantum coherences, the user may shift a set of movable vertical lines ('crosshairs'): a single crosshair and a pair of crosshairs can be adjusted to the central peak and the peak doublet, respectively. Corresponding crosshairs in different strips are automatically readjusted, so that the precise match of the corresponding peak positions of 309 and 310 becomes readily apparent. Please note that the spectral widths along ω_1 vary among the different 3D experiments. The current chemical shifts are given in a small window (indicated with 'chemical shifts'). The user may also display selected regions from 2D spectra, e.g. the region from a 2D [^{13}C,^{1}H]-COSY that comprises the cross peak of the CH^{α} group of 309. The cursor in this window ('13C1H-cosy') is automatically adjusted according to the current chemical shifts extracted from the 3D spectra. A description of SPSCAN is available via http://www.mol.biol.ethz.ch/wuthrich/software/spscan/.

search for sequential neighbours within sets of [ω_1, ω_3]-strips (Figure 4): for each strip one obtains a string of the remaining strips ranked according to a scoring function. This function weights differences between $^{13}C^{\alpha}/^{1}H^{\alpha}$ chemical shifts derived from two strips, $\Delta\Omega$, according to $\exp\{-(\Delta\Omega/\Delta\Omega_{ref})^2\}$, where $\Delta\Omega_{ref}$ is a parameter that has to be adapted to the spectral resolution. For the present study, $\Delta\Omega_{ref}$ was set to 16 Hz and 26 Hz for intra- and interspectral comparisons, respectively. A putative match of a sequential and an intraresidual connectivity is considered by multiplying the exponential term with a user-definable factor, e.g. 4 in the present study.

In order to use a 3D HNN<CO,CA> spectrum for the interactive sequential assignment protocol including visual comparison of peak positions, SPSCAN offers a routine to transform the 3D HNN<CO,CA> spectrum into a pseudo-3D HNNCA spectrum. The [$\omega_1(^{13}C)$, $\omega_3(^{1}H^{N})$] strips are symmetrized along $\omega_1(^{13}C)$ about the central peak at $\Omega(^{13}C{=}O)$ and are separately recalibrated, so that the central peaks are positioned at the apparent $^{13}C^{\alpha}$ carrier position. After scaling the ω_1-axis with $1/\kappa$, the strips are written in the form of the pseudo-spectrum which can be handled by XEASY. Due to the very high signal-to-noise ratio quite generally observed for the central peaks (see also Figure 4 in Szyperski et al., 1995), additional manual input is rarely required.

Results and Discussion

To demonstrate the use of projected 4D spectra recorded with simultaneous acquisition of central peaks, we acquired the above described spectra for the 6.7 kDa N-terminal 63-residue fragment of the 434 repressor (434(1–63)) (Neri et al., 1992b). The NMR measurements were performed at the relatively low temperature of 13 °C, where 434(1–63) reorients with a correlation time of about 6 ns (Luginbühl et al., 1997). This is typical for proteins with a molecular weight of about 15 kDa at commonly used temperatures around 30 °C, so that the signal-to-noise ratio of the spectral data presented here is readily attainable also for medium sized proteins. Table 2 affords a survey of the number of scalar connectivities that were observed. The nearly complete yield provided a sound basis for obtaining sequence specific assignments, and the large number of automatically identified connectivities offered a convenient starting point for the rapid interactive completion of the peak picking procedure. In particular, the parameter of the peak picking routine was adjusted for a 'conservative' search, i.e., there were no automatically picked peaks that had to be removed during the manual completion of the search. Table 3 shows that the subsequent automatic identification of sequential neighbours was highly efficient: the actual sequential neighbour was within the first four strips proposed by SPSCAN for all residues. A table with the ^{13}C chemical shift assignments is available from the authors.

Sequential assignment with 3D HNN<CO,CA>

Since 3D HNN<CO,CA> provides sequential connectivities (Figure 1A), the assignment of smaller proteins may be performed with 3D HNN<CO,CA> alone. Since $\Omega(^{13}C^{\alpha})$ is encoded in the in-phase splitting of doublets centered about $\Omega(^{13}C{=}O)$ (Szyperski et al., 1995) the sequential assignment has to rely on the comparison of the splittings (Figure 5A). However, for visual inspection it is preferable to work with the pseudo-3D HNNCA spectrum (Figure 5B). All sequential connectivities could be observed (Table 2), but due to the poor chemical shift dispersion of the purely α-helical protein 434(1–63) (Neri et al., 1992c) it was not possible to distinguish the two tripeptide segments Glu 32-Gln 33-Leu 34 and Arg 43-Phe 44-Leu 45 (Table 3).

Sequential assignment with 3D HNNCAHA

3D HNNCAHA may likewise suffice to sequentially assign smaller proteins. Due to an additional magnetization transfer from $^{13}C^{\alpha}$ to $^{1}H^{\alpha}$ and an extended time period with transverse $^{13}C^{\alpha}$ magnetization, its sensitivity is reduced relative to 3D HNN<CO,CA>. However, the sequential assignment with 3D HNNCAHA is based on two chemical shifts which makes its use obviously more efficient. We observed the majority of sequential connectivities (Table 2) which allowed to assign (Table 3) the backbone resonances of $^{1}H^{N}$, ^{15}N, $^{13}C^{\alpha}$ and $^{1}H^{\alpha}$ in the straightforward fashion exemplified in Figure 6: the negative central peaks provide the $^{13}C^{\alpha}_{i-1} \rightarrow {}^{1}H^{N}_{i}$ and the positive doublets yield also the $^{1}H^{\alpha}_{i-1} \rightarrow {}^{1}H^{N}_{i}$ connectivities.

Sequential assignment with 3D HNN<CO,CA> and 3D H$^{\alpha/\beta}$C$^{\alpha/\beta}$(CO)NHN

For medium-sized proteins, an incomplete set of sequential connectivities will usually be registered in 3D HNN<CO,CA>. However, provided that the $^{13}C^{\alpha}$ chemical shift dispersion is sufficient, one

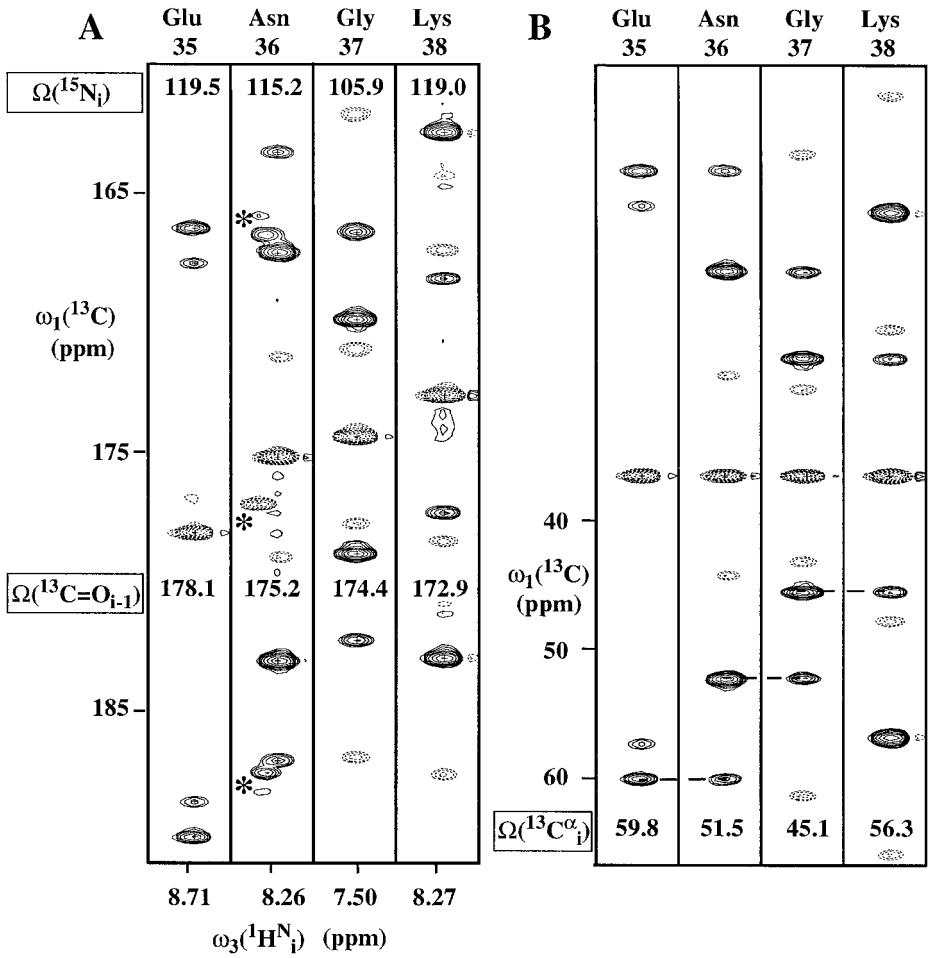

Figure 5. (A) Contour plot of [$\omega_1(^{13}C)$, $\omega_3(^1H^N)$]-strips from a 3D HNN<CO,CA> spectrum recorded with a 1.5 mM sample of 434(1–63) in 90% H_2O/10% D_2O (pH = 4.5 and T = 13 °C). Dashed and solid contour lines represent negative and positive peaks, respectively. The strips were taken at the ^{15}N chemical shifts (indicated at the top) of the residues 35–38 and are centered about their $^1H^N$ chemical shifts. The sequence-specific assignments of the amide chemical shifts are indicated at the top of each strip and are referred to as i. $\Omega(^{13}C{=}O_{i-1})$ is given by the central negative peak in strip i and is indicated, and $\Omega(^{13}C^{\alpha}_{i})$ and $\Omega(^{13}C^{\alpha}_{i-1})$ are extracted from the positive peak doublets (see Figure 1). Negative peaks of low intensity correspond to doublets of doublets arising from modulation of the transfer amplitude with both $\Omega(^{13}C^{\alpha}_{i-1})$ and $\Omega(^{13}C^{\alpha}_{i})$ (Szyperski et al., 1995). ^1H and ^{13}C chemical shifts are in ppm relative to 2,2-dimethyl-2-silapentane-5-sulfonate sodium salt (DSS); the ^{13}C chemical shifts are calculated with $\Xi(^{13}C/^1H) = 0.251449530$ (Wishart et al., 1995). The spectrum was recorded on a Bruker AMX 600 spectrometer, and $121(t_1) \times 45(t_2) \times 512(t_3)$ complex points were accumulated with $\kappa = 0.5$, so that $t_{1max}(^{13}C{=}O) = 16.9$ ms; $t_{1max}(^{13}C^{\alpha}) = 8.45$ ms; $t_{1max}(^{15}N) = 31.9$ ms; $t_{3max}(^1H^N) = 62.5$ ms. The $^{13}C^{\alpha}$ carrier was set to 53 ppm and shifted to an apparent position at 36.5 ppm employing TPPI (Marion and Wüthrich, 1983; Szyperski et al., 1995). The acquisition was started with the sixth complex point and the first five points were then obtained by linear prediction (Stephenson, 1988) to achieve zero first-order phase correction along ω_1. Two scans per increment were acquired and the sensitivity enhancement scheme of Palmer et al. (1991) was applied, resulting in a total measurement time of 27 h. The data matrix was extended by linear prediction along t_1 and t_2, and then multiplied with a cosine window in t_1 and t_2, and a sine window shifted by 60 °C in t_3 (DeMarco and Wüthrich, 1976). The digital resolution after zero-filling was 15 Hz along $\omega_1(^{13}C)$, 22 Hz along $\omega_2(^{15}N)$ and 8 Hz along $\omega_3(^1H^N)$. The spectrum was processed using the program PROSA (Güntert et al., 1992). (B) The same strips as in (A) taken from the pseudo-3D HNNCA spectrum: after symmetrization about the central peaks at $\Omega(^{13}C{=}O_{i-1})$ the strips were shifted upfield so that the central peak is positioned at to the apparent $^{13}C^{\alpha}$ carrier position (36.5 ppm). The symmetrization was performed by replacing the intensities of each pair of data points i and j, centered about the maximum of the central peaks, by $\mathrm{sgn(i)} \cdot \min(|i|, |j|)$ in the case i and j have the same sign and by zero otherwise. This eliminates peaks from other residues with very similar or identical ^{15}N and $^1H^N$ chemical shifts: the peaks of Leu 60 (marked with asterisks) in the strip of Asn 36 in (A) are not present in the corresponding strip shown in (B). The ω_1-axis is scaled up by a $1/\kappa = 2$ relative to (A) so that $\Omega(^{13}C^{\alpha})$ can be read off the ω_1-axis. $\Omega(^{13}C^{\alpha}_{i})$ is indicated at the bottom of strip i.

Table 2. Experimentally observed and automatically identified scalar connectivities in 434(1–63)[a]

Experiment	Type of connectivity $^1H_i^N \rightarrow$	Experimentally observed[b]	Automatically identified with the peak picking routine of SPSCAN[c]
3D HNN<CO,CA>	$^{13}C{=}O_{i-1}$:	60/60 (100%)[d]	60 (100%)
	$^{13}C_i^{\alpha}$:	60/60 (100%)[d]	60 (100%)
	$^{13}C_{i-1}^{\alpha}$:	60/60 (100%)[d]	58 (97%)
3D HNNCAHA	$^{13}C_i^{\alpha}$:	60/60 (100%)[d]	58 (97%)
	$^1H_i^{\alpha}$:	63/64 (98%)[e]	61 (97%)
	$^{13}C_{i-1}^{\alpha}$:	57/60 (95%)[d]	45 (79%)
	$^1H_{i-1}^{\alpha}$:	56/64 (88%)[e]	41 (73%)
3D $H^{\alpha/\beta}C^{\alpha/\beta}$(CO)NHN	$^{13}C_{i-1}^{\alpha}$:	60/60 (100%)[d]	60 (100%)
	$^{13}C_{i-1}^{\beta}$:	54/55 (98%)[f]	52 (95%)
	$^1H_{i-1}^{\alpha}$:	64/64 (100%)[e]	64 (100%)
	$^1H_{i-1}^{\beta}$:	76/80 (95%)[g]	65 (86%)

[a] T = 13 °C; protein concentration = 1.5 mM; measurement times: 27 h, 15 h and 22 h for 3D HNN<CO,CA>, 3D HNNCAHA and 3D $H^{\alpha/\beta}C^{\alpha/\beta}$(CO)NHN, respectively.

[b] The expected number of connectivities was calculated on the basis of the known ^1H resonance assignments (Neri et al., 1992c): two resolved ^1H connectivities are expected for $^{\alpha}CH_2$ groups of glycyls and $^{\beta}CH_2$ groups with ^1H chemical shift differences larger than 0.1 ppm.

[c] The fraction of connectivities identified with SPSCAN is calculated relative to the corresponding number of experimentally observed connectivities.

[d] Expected number: 63 residues minus two prolyls minus one N-terminal residue (60).

[e] Expected number: number calculated for footnote 'd' plus four (out of five) glycyl residues with non-degenerate $^1H^{\alpha}$ chemical shifts (64).

[f] Expected number: number calculated for footnote 'd' minus five glycyl residues (55).

[g] Expected number: number calculated for footnote 'f' plus number of residues with two non-degenerate β-proton chemical shifts (80).

Table 3. Semi-automatic sequential assignment of 434(1–63)

3D experiments	Fraction of actual sequential neighbours that were attributed to[a]			Fraction of residues sequentially assigned by inspection of the ranking maps of SPSCAN[b]
	rank = 1	rank = 2–4	rank > 4	
HNN<CO,CA>	47/57 (82%)	10 (18%)	0	57/63 (90%)
HNNCAHA	50/57 (88%)	7 (12%)	0	63/63 (100%)
HNN<CO,CA> / $H^{\alpha/\beta}C^{\alpha/\beta}$(CO)NHN	49/57 (86%)	8 (14%)	0	63/63 (100%)
HNNCAHA / $H^{\alpha/\beta}C^{\alpha/\beta}$(CO)NHN	57/57 (100%)	0	0	63/63 (100%)

[a] Three out of 60 (ω_1, ω_3)-strips are either sequential neighbours of a prolyl residue or represent a terminal residue. Hence, the fraction is referred to a total of 57.

[b] The two prolyl residues and the N-terminal residue were included for the total number of residues, since their CH^{α}-CH_2^{β} moieties can be assigned via sequential connectivities. Hence, the fraction is referred to a total of 63.

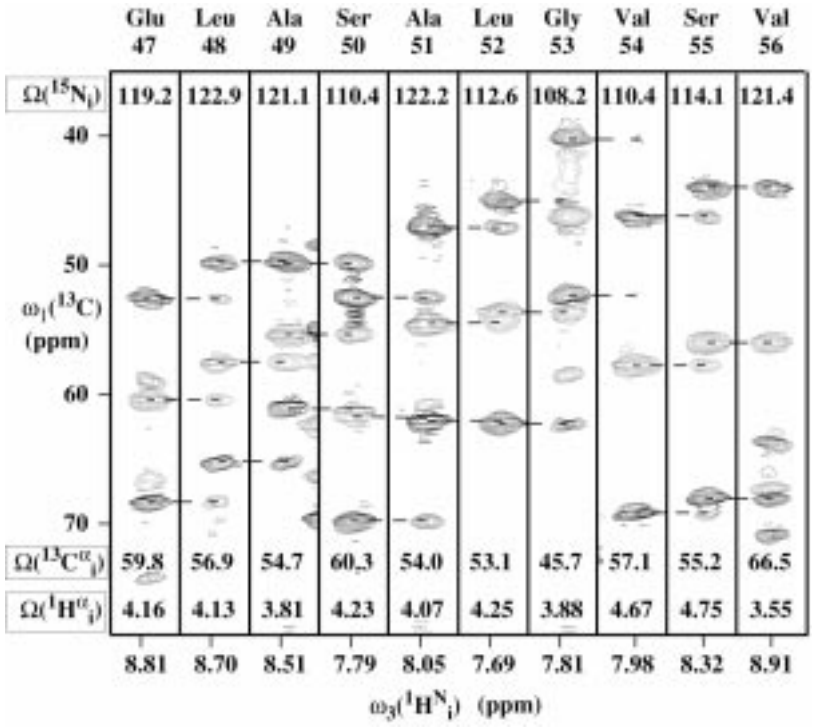

Figure 6. Contour plot of $[\omega_1(^{13}C), \omega_3(^1H^N)]$-strips taken from the 3D HNN<u>CAHA</u> spectrum. The strips were taken at the ^{15}N chemical shifts (indicated at the top) of residues 47 to 56. The sequence-specific resonance assignments of the amide chemical shifts are given at the top of each strip and are referred to as i. Dashed and solid contour lines represent negative and positive peaks, respectively, and the sequential connectivities are indicated by dashed lines. $\Omega(^{13}C_i^\alpha)$ is given by the negative central peaks and $\Omega(^1H_i^\alpha)$ is extracted from the positive peak doublets (see Figure 1). $\Omega(^{13}C_i^\alpha)$ and $\Omega(^1H_i^\alpha)$ are indicated at the bottom of strip i. The spectrum was recorded on a Bruker AMX 600 spectrometer. $51(t_1) \times 30(t_2) \times 512(t_3)$ complex points were accumulated with $\kappa = 1.70$, so that $t_{1,max}(^{13}C^\alpha) = 6.50$ ms, $t_{1,max}(^1H^\alpha) = 11.1$ ms, $t_{2,max}(^{15}N) = 21.0$ ms and $t_{3,max}(^1H^N) = 62.5$ ms. Four scans per increment were recorded and a sensitivity enhancement scheme (Palmer et al., 1991) was applied, resulting in a measurement time of about 15 h. Prior to Fourier transformation the data matrix was extended by linear prediction along t_1 and t_2, respectively, and multiplied with a cosine-squared window in t_1 and t_2, and a sine window shifted by 60° in t_3 (DeMarco and Wüthrich, 1976). The digital resolution after zero-filling was 32 Hz along $\omega_1(^{13}C/^1H)$, 22 Hz along $\omega_2(^{15}N)$ and 8.0 Hz along $\omega_3(^1H^N)$.

may supplement 3D HNN<u>CO</u>,<u>CA</u>> with an experiment tailored to observe sequential connectivities, e.g. 3D $\underline{H}^{\alpha/\beta}\underline{C}^{\alpha/\beta}$(CO)NHN (Szyperski et al., 1994a). We observed all correlations expected for 3D $\underline{H}^{\alpha/\beta}\underline{C}^{\alpha/\beta}$(CO)NHN, except for a few originating from CH_2^β-groups (Table 2). Hence, the sequential assignment could be performed as shown in Figure 7. Subspectrum II of the 3D $\underline{H}^{\alpha/\beta}\underline{C}^{\alpha/\beta}$(CO)NHN experiment provides $^{13}C^\alpha_{i-1} \rightarrow {}^1H^N_i$ connectivities. These can be matched with the intraresidual 3D $^{13}C^\alpha_i \rightarrow {}^1H^N_i$ connectivities observed in the 3D HNN<u>CO</u>,<u>CA</u>> spectrum or in the corresponding pseudo-3D HNNCA spectrum. Having all chemical shifts of the CH^α-CH^β_n moieties, the identification of the amino acid type is greatly facilitated (Wüthrich, 1976). Hence, the chemical shifts of all polypeptide spins, except for four $^1H^\beta$ resonances and those of the peripheral side chain nuclei beyond $C^\beta H_n$, could be obtained from only two triple resonance NMR experiments (Table 3).

Sequential assignment with 3D HNN<u>CAHA</u> and 3D $\underline{H}^{\alpha/\beta}\underline{C}^{\alpha/\beta}$(CO)NHN

If $^{13}C^\alpha$ chemical shift degeneracy cannot be overcome by chemical shift-based identification of the amino acid residue type, the combined use of 3D HNN<u>CAHA</u> and 3D $\underline{H}^{\alpha/\beta}\underline{C}^{\alpha/\beta}$(CO)NHN is advantageous (Figure 8). The central peaks in subspectrum II of the 3D $\underline{H}^{\alpha/\beta}\underline{C}^{\alpha/\beta}$(CO)NHN experiment provide $^{13}C^\alpha_{i-1} \rightarrow {}^1H^N_i$ connectivities, while the doublets of subspectrum I also yield $^1H^\alpha_{i-1} \rightarrow {}^1H^N_i$ connectivities. Hence, comparison with the negative central peaks and positive doublets in the 3D HNN<u>CAHA</u> allows to order the $[\omega_1, \omega_3]$-strips of the two spectra sequentially.

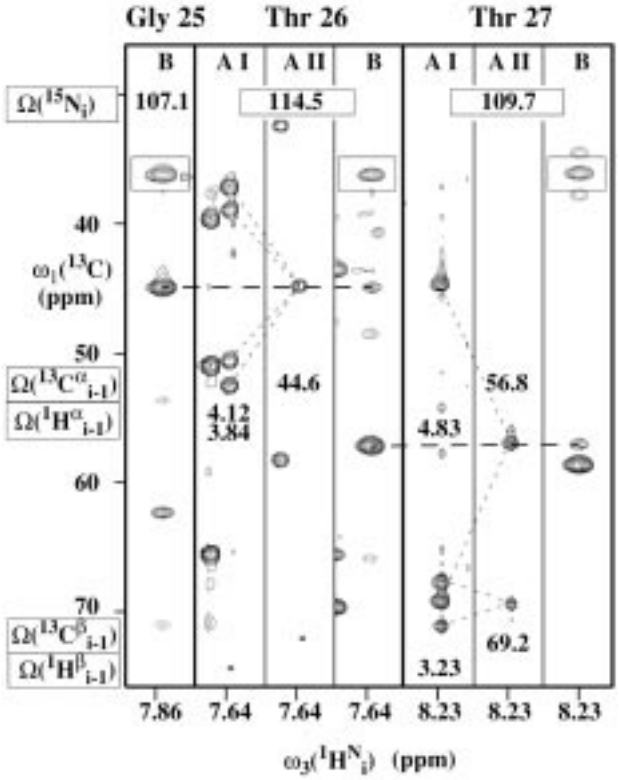

Figure 7. Contour plot of [$\omega_1(^{13}C)$, $\omega_3(^1H^N)$]-strips taken from subspectrum I (strips labeled with AI) and subspectrum II (strips labeled with AII) of the 3D $\underline{H}^{\alpha/\beta}\underline{C}^{\alpha/\beta}$(CO)NHN experiment, and from the pseudo-3D HNNCA spectrum (strips labeled with B). The strips were taken at the ^{15}N chemical shifts (indicated at the top) of residues 25 to 27. The sequence-specific resonance assignments of the amide chemical shifts are given at the top of each strip and are referred to as i. $\Omega(^1H^{\alpha/\beta}_{i-1})$ and $\Omega(^{13}C^{\alpha/\beta}_{i-1})$ obtained from 3D $\underline{H}^{\alpha/\beta}\underline{C}^{\alpha/\beta}$(CO)NHN are given in the strips AI and AII of residue i. Corresponding peak doublets in AI and central peaks in AII are connected by dotted lines. The central peaks of 3D HNN<CO,CA> are indicated in boxes in the pseudo-3D HNNCA spectrum. Dashed and solid contour lines represent negative and positive peaks, and sequential connectivities are indicated by dashed lines. For the details of the 3D HNN<CO,CA> experiment see the legend of Figure 5. The 3D $\underline{H}^{\alpha/\beta}\underline{C}^{\alpha/\beta}$(CO)NHN experiment was accumulated with $82(t_1) \times 30(t_2) \times 512(t_3)$ complex points with $\kappa = 1.70$, so that $t_{1max}(^1H^{\alpha/\beta}) = 11.2$ ms; $t_{1max}(^{13}C^{\alpha/\beta}) = 6.56$ ms; $t_{2max}(^{15}N) = 21.0$ ms; $t_{3max}(^1H^N) = 62.5$ ms. The two data sets required for the acquisition of central peaks were accumulated in an interleaved fashion. For each data set two scans per increment were acquired and a sensitivity enhancement scheme (Palmer et al., 1991) was applied, resulting in a total measurement time of about 22 h. Prior to Fourier transformation the data matrix was extended by linear prediction along t_1 and t_2, and multiplied with a cosine window in t_1 and t_2, and a sine window shifted by 70° in t_3 (DeMarco and Wüthrich, 1976). The digital resolution after zero-filling was 24 Hz along $\omega_1(^{13}C/^1H)$, 22 Hz along $\omega_2(^{15}N)$, and 8.0 Hz along $\omega_3(^1H^N)$.

Except for one $^1H^{\alpha}_{i-1} \rightarrow {}^1H^N_i$ connectivity, a complete set of sequential connectivities was registered (Table 2) yielding a nearly complete sequential resonance assignment of the CH^{α}-CH^{β} moieties (Table 3).

Comparison of spectral resolution: Projected versus conventional 4D experiments

Table 4 provides key parameters chosen for the implementations of our 3D HNN<u>CAHA</u> spectrum and three representative 4D HNNCAHA / 4D HACANHN spectra (Boucher et al., 1992b; Kay et al., 1992; Constantine et al., 1993; Gooley et al., 1993; Moy et al., 1994; Hardman et al., 1995), and affords parameters for their comparison (see Appendix). Most important, the average maximal evolution times in the indirect dimensions, θ_{av}, are much shorter in the 4D spectra, although they were recorded with a larger total number of complex points in the indirect dimensions. Recording of a projected 3D HNN<u>CAHA</u> experiment with the data sizes of the 4D spectra and setting $\kappa = {}^{4D}t_{max}(^1H^{\alpha})/{}^{4D}t_{max}(^{13}C^{\alpha})$ would result in a relative increase of t_{max}, ϵ, between 5.3 and 13 (Table 4). This corresponds to hypothetical $t_{max}(^1H^{\alpha})$ and $t_{max}(^{13}C^{\alpha})$ values between 14 ms and 137 ms, and between 14 ms and 69 ms, respectively. Due to transverse relaxation and passive scalar couplings, such

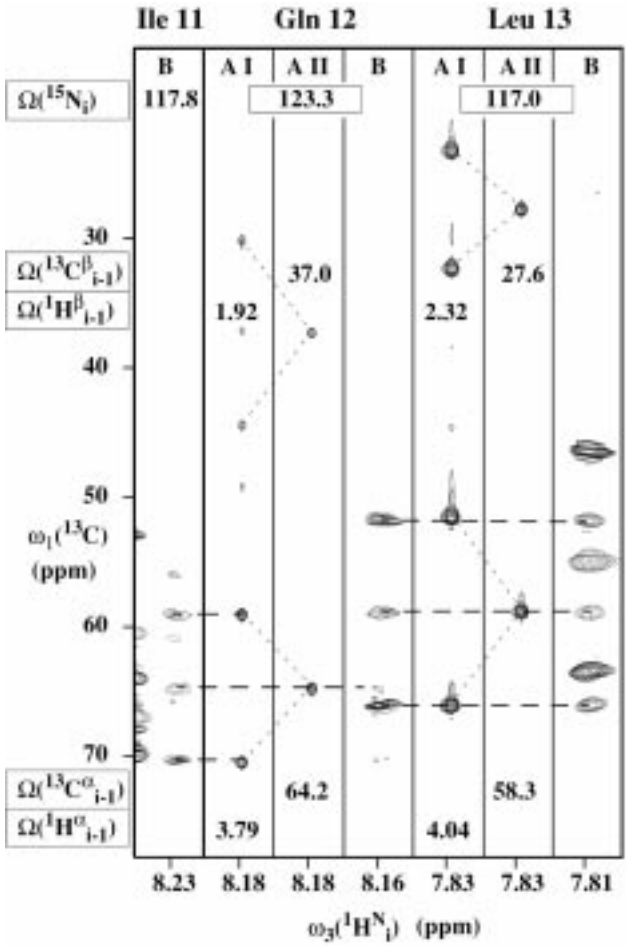

Figure 8. Contour plot of $[\omega_1(^{13}C), \omega_3(^1H^N)]$-strips taken from subspectrum I (strips labeled with AI) and subspectrum II (strips labeled with AII) of the 3D $\underline{H}^{\alpha/\beta}\underline{C}^{\alpha/\beta}$(CO)NHN experiment, and from 3D HNN<u>CAHA</u> (strips labeled with B). The strips were taken at the ^{15}N chemical shifts (indicated at the top) of residues 11 to 13. The sequence-specific resonance assignments of the amide chemical shifts are given at the top of each strip and are referred to as i. $\Omega(^1H^{\alpha/\beta}_{i-1})$ and $\Omega(^{13}C^{\alpha/\beta}_{i-1})$ obtained from 3D $\underline{H}^{\alpha/\beta}\underline{C}^{\alpha/\beta}$(CO)NHN are given in the strips AI and AII of residue i. Corresponding peak doublets in AI and central peaks in AII are connected by dotted lines. Dashed and solid contour lines represent negative and positive peaks, respectively, and sequential connectivities are indicated by dashed lines. For the details of the 3D $\underline{H}^{\alpha/\beta}\underline{C}^{\alpha/\beta}$(CO)NHN and 3D HNN<u>CAHA</u> experiments see the legends of Figures 7 and 6, respectively.

long maximal evolution times do not enhance the resolution in practice. Consequently, the gain achieved upon projection can partly be invested to increase $t_{max}(^{15}N)$: we could afford a $t_{max}(^{15}N)$ value in 3D HNN<u>CAHA</u> which is two to three times larger than that for the 4D experiments (Table 4).

Alternatively, we may ask for the measurement time required to achieve the maximal evolution times of our 3D HNN<u>CAHA</u> spectrum with the implementations of 4D experiments. Therefore, the data size of the 4D experiments had to be extended to ^{4Dex}d complex points in the indirect dimensions (see Appendix). The resulting hypothetical data sets are at least an order of magnitude larger than that of a 3D HNN<u>CAHA</u> experiment recorded with the same sweep width, and the minimal demand of instrument time scales up with the same factor (Table 4). In view of the ongoing rapid increase in spectrometer performance and the fact that the option for a minimal two- or four-step phase cycle and for the application of a sensitivity enhancement scheme (e.g. Palmer et al., 1991) should be retained, recording of projected 4D spectra thus appears to be more efficient than acquiring the parent counterparts.

Table 4. Comparison of 3D HNNCAHA with 4D HNNCAHA and 4D HACANHN[a]

Experiment	$t_{max}(^1H^\alpha)$ $\theta(^1H^\alpha)$	$t_{max}(^{13}C^\alpha)$ $\theta(^{13}C^\alpha)$	$t_{max}(^{15}N)$ $\theta(^{15}N)$	θ_{av}	Increments[b] Data size	m_{min}	ϵ	^{4Dex}d Data size	$^{4Dex}m_{min}$
3D HNNCAHA	11.1 ms 1.00	6.50 ms 1.00	22.3 ms 1.00	1.00	52×30 25.5 MB[c]	1.8 h		– –	–
4D HACANHN[d]	12.8 ms 1.15	4.8 ms 0.73	10.0 ms 0.45	0.78	$32 \times 12 \times 10$ 126 MB[c]	8.5 h	10.1	$28 \times 16 \times 22$ 323 MB[c]	22 h
4D HACANHN[e]	10.5 ms 0.95	5.3 ms 0.82	7.9 ms 0.35	0.71	$32 \times 16 \times 8$ 134 MB[c]	9.1 h	13	$36 \times 20 \times 23$ 543 MB[c]	37 h
4D HNNCAHA[f]	2.67 ms 0.24	2.56 ms 0.39	8.0 ms 0.36	0.33	$8 \times 8 \times 16$ 33.5 MB[c]	2.3 h	5.3	$32 \times 21 \times 44$ 969 MB[c]	66 h

[a] The values for θ_{av}, m_{min}, ϵ, ^{4Dex}d, and $^{4Dex}m_{min}$ have been calculated with Equations (A7), (A9), (A5), (A8) and (A9) of the Appendix, respectively.
[b] The two numbers given for 3D HNCAHA correspond to l and m, and the three numbers given for the 4D spectra correspond to i, j and k as introduced in Equations (A5), (A8), and (A9).
[c] With 512 complex points in the acquisition domain.
[d] From Boucher et al. (1992).
[e] From Hardman et al. (1995).
[f] From Kay et al. (1992).

Comparison of sensitivity: 3D HNNCAHA versus 3D HNNCACB

When invoking $^1H^\alpha$ or $^{13}C^\beta$ chemical shifts to resolve assignment ambiguities arising from $^{13}C^\alpha$ chemical shift degeneracy (Table 1), 3D HNNCAHA and 3D HNNCACB overtake an analogous role since both provide the intraresidual connectivities. For transverse relaxation times being typical for proteins of 15–20 kDa, i.e., $T_2(^1H^\alpha) = T_2(^{13}C^\alpha) = 15$ ms and $T_2(^1H^N) = T_2(^{15}N) = 50$ ms, the efficiencies for the intraresidual transfers $^1H_i^N \rightarrow {}^1H_i^\alpha$ and $^1H_i^N \rightarrow {}^{13}C_i^\alpha$ and the sequential transfers $^1H_i^N \rightarrow {}^1H_{i-1}^\alpha$ and $^1H_i^N \rightarrow {}^{13}C_{i-1}^\alpha$ can be calculated for 3D HNNCAHA using Equations (1) and (2). With $t_1 = 0$ ms one obtains 0.024, 0.036, 0.006 and 0.009, respectively, where the first and third value representing $^1H_i^N \rightarrow {}^1H_i^\alpha$ and $^1H_i^N \rightarrow {}^1H_{i-1}^\alpha$ have been divided by 2, because these transfers yield peak doublets. Calculating the net efficiencies for 3D HNNCACB with the same relaxation times and the parameters of Wittekind and Müller (1993), one obtains 0.026, 0.024, 0.007 and 0.006 for $^1H_i^N \rightarrow {}^{13}C_i^\alpha$, $H_i^N \rightarrow {}^{13}C_i^\beta$, $H_i^N \rightarrow {}^{13}C_{i-1}^\alpha$ and $H_i^N \rightarrow {}^{13}C_{i-1}^\beta$, respectively. Hence, the intensity expected for each peak of the intraresidual doublet in 3D HNNCAHA, which itself encodes both intraresidual correlations, is expected to be of the same intensity as the peak representing the intraresidual correlation in 3D HNNCACB. Moreover, in 3D HNNCAHA we exploit axial peak magnetization to detect central peaks having about the same intensity as the doublet components. This allows to symmetrize the 3D HNNCAHA spectrum, increasing its signal-to-noise ratio. Hence, 3D HNNCAHA exhibits a sensitivity which is at least comparable to 3D HNNCACB, although we have decided to compromise on τ_4 to observe also glycyls. This is because $^1J\{^{13}C^\alpha, ^1H^\alpha\} >> J\{^{13}C^\alpha, ^{13}C^\beta\}$, so that transverse magnetization resides on $^{13}C^\alpha$ for 14.2 ms in 3D HNNCACB (Wittekind and Müller, 1993) but only for 4.0 ms in 3D HNNCAHA.

Conclusions

The backbone resonances of smaller proteins can be assigned using either 3D HNN<CO,CA> or 3D HNNCAHA, and when working with proteins with a molecular weight up to about 15 kDa these experiments are neatly complemented by 3D $H^{\alpha/\beta}C^{\alpha/\beta}$(CO)NHN. The high yields of the automatically performed steps (Tables 2 and 3) were due to the detection of central peaks (Figure 1) and spectral resolutions being typical for conventional 3D experiments. Hence, relatively tight match tolerances of the chemical shifts could be used for the search of sequentially neighbouring strips. Clearly, spectral overlap

increases for a medium-sized protein when compared with 434(1–63). However, proteins exhibit quite generally good $^{1}H^{N}$ and ^{15}N chemical shift dispersion, and it is thus of prime importance that projected 4D experiments are feasible with long maximal evolution times in the indirect ^{15}N dimension (Table 4). Moreover, the acquisition of central peaks restores the dispersion of the parent 4D experiment. This feature hardly facilitated the assignment of 434(1–63) (Figure 5), but it was of importance for the assignment of medium-sized proteins, e.g. the 21 kDa protein FimC (Pellecchia et al., 1998). Projected 4D triple resonance experiments thus appear to be highly efficient for assigning medium-sized proteins.

One may then devise a minimal set of six experiments delineating exclusively scalar connectivities for such proteins: 3D $\underline{H}^{\alpha/\beta}$ $\underline{C}^{\alpha/\beta}$(CO)NHN and 3D HNN<CO,CA> provide the chemical shifts of all polypeptide spins except for the peripheral side chain nuclei beyond $C^{\beta}H_n$, 3D HC(C)H-COSY (Kay et al., 1990b), or 2D HC(C)H-COSY for small proteins (Szyperski et al., 1997), yield the assignment of the peripheral aliphatic spins beyond $C^{\beta}H_n$, 2D $(H^{\beta})C^{\beta}(C^{\gamma}C^{\delta})H^{\delta}$ (Yamazaki et al., 1993) provides the connection of aromatic $^{13}C^{\beta}$ and H^{δ} spins, and 3D ^{1}H-TOCSY-relayed ct-[^{13}C,^{1}H]-HMQC and 2D (H)C(C)H-TOCSY (Zerbe et al., 1996) allow to identify the aromatic spin systems. This set of experiments is in principle sufficient for the complete resonance assignment, excluding only the side chain NH_n moieties, the quaternary aromatic carbons and the CH^{ϵ} groups of the histidinyls. According to our experience, about one week of measurement time suffices to record all experiments with a 1–2 mM sample (the spectra of the present study were recorded in about 2.5 days). Furthermore, triple resonance experiments are usually employed in conjunction with NOESY, and it is then likely that NOESY resolves remaining ambiguities. In addition, the backbone ^{13}C=O resonance assignments provide a suitable basis to employ 3D ^{13}C=O resolved [^{1}H-^{1}H]-NOESY-H(N)CO (Zhang et al., 1996).

The 4D peak lists derived from the projected experiments might also be introduced into a program for automated sequence-specific assignment (e.g. Zimmerman and Montelione, 1995). In particular, the program ALPS (Morelle et al., 1995) has been written for the automated sequential assignment using peak lists from a set of seven reduced-dimensionality 2D experiments as input, thereby relying on both $^{1}H^{\alpha}$ and ^{13}C=O chemical shifts to overcome $^{13}C^{\alpha}$ chemical shift degeneracy. Since these experiments were recorded without simultaneous acquisition of central peaks (Brutscher et al., 1994, 1995a) their position had to be taken from 2D [^{15}N, ^{1}H]-HSQC, which introduces an additional experimental uncertainty for the identification of the doublets. Moreover, the gain in resolution obtainable upon projection is usually limited by passive scalar couplings. For example, $^{1}J\{^{13}C^{\alpha}, ^{13}C^{\beta}\} = 35$ Hz restricts the maximal evolution time of $^{13}C^{\alpha}$ in HNNCA to values below 14 ms, which is routinely achieved in conventional 3D experiments. Hence, one can usually not take advantage of a potentially very large resolution enhancement when reducing the dimensionality from three to two. For smaller molecules, projected constant-time experiments involving several dephasing/rephasing cycles can be devised that effectively decouple the scalar interaction (Szyperski et al., 1997). However, this will usually lead to an unacceptable reduction in sensitivity for macromolecules. It thus appears that for the assignment of medium-sized proteins, the projection of 4D experiments makes the better use of the potentialities of the reduced-dimensionality approach (Szyperski et al., 1993b).

In contrast to published 4D schemes (Boucher et al., 1992a,b; Kay et al., 1992; Olejniczak et al., 1992), 3D HNNCAHA allows for the detection of glycyls. This is of key importance for the assignment of proteins with glycyl-rich segments, and 3D HNNCAHA / 3D $\underline{H}^{\alpha/\beta}\underline{C}^{\alpha/\beta}$(CO)NHN thus provide the same yield of sequential connectivities as 3D HNNCACB / 3D CBCA(CO)NHN, i.e., only prolyls interrupt the sequential assignment. For larger proteins (> 15–20 kDa) we suggest to employ 3D HNNCAHA in conjunction with 3D HACA(CO)NHN, which is expected to be more sensitive than 3D $\underline{H}^{\alpha/\beta}\underline{C}^{\alpha/\beta}$(CO)NHN. Our calculations of transfer amplitudes indicate that 3D HNNCAHA compares favourably with 3D HNNCACB in terms of sensitivity. This is also supported by the survey of 'first-scan-sensitivities' reported by Buchler et al. (1997) showing that for larger proteins HNNCAHA is expected to be more sensitive than HNNCACB. Since triple resonance experiments providing the intraresidual connectivities constitute quite generally the 'bottle-neck' for obtaining sequential assignments, 3D HNNCAHA / 3D HACA(CO)NHN promises to be a viable alternative to 3D HNNCACB / 3D CBCA(CO)NHN.

Acknowledgements

Financial support was obtained from the Schweizerischer Nationalfonds (project 31.49047.96). B.B. and R.W.G are indebted to the European Molecular Biology Organization (EMBO) and the Deutsche Forschungsgemeinschaft (DFG), respectively, for a scholarship. We thank Kurt Wüthrich for the careful reading of the manuscript, constructive criticism and continuous support.

References

Bartels, C., Xia, T.H., Billeter, M., Güntert, P. and Wüthrich, K. (1995) *J. Biomol. NMR*, **6**, 1–10.

Bartels, C., Billeter, M., Güntert, P. and Wüthrich, K. (1996) *J. Biomol. NMR*, **7**, 207–213.

Baumann, R., Anil Kumar, Ernst, R.R. and Wüthrich, K. (1981) *J. Magn. Reson.*, **44**, 76–83.

Bax, A. and Ikura, M. (1991) *J. Biomol. NMR*, **1**, 99–104.

Bax, A. and Pochapsky, S. (1992) *J. Magn. Reson.*, **99**, 638–643.

Bodenhausen, G. and Ruben, D. (1980) *Chem. Phys. Lett.*, **69**, 185–188.

Boucher, W., Laue, E.D., Campbell-Burk, S.L. and Domaille, P.J. (1992a) *J. Am Chem. Soc.*, **114,** 2262–2264.

Boucher, W., Laue, E.D., Campbell-Burk, S.L. and Domaille, P.J. (1992b) *J. Biomol. NMR*, **2**, 631–637.

Bracken, C., Palmer III, A.G. and Cavanagh, J. (1997) *J. Biomol. NMR*, **9**, 94–100.

Brutscher, B., Simorre, J.P., Caffrey, M.S. and Marion, D. (1994) *J. Magn. Reson.*, **B105**, 77–82.

Brutscher, B., Cordier, F., Simorre, J.P., Caffrey, M. and Marion, D. (1995a) *J. Biomol. NMR*, **5**, 202–206.

Brutscher, B., Morelle, N., Cordier, F. and Marion, D. (1995b) *J. Magn. Reson.*, **B105**, 238–242.

Buchler, N.E.G., Zuiderweg, E.R.P., Wang, H. and Goldstein, R.A. (1997) *J. Magn. Reson.*, **125**, 34–42.

Cavanagh, J. and Rance, M. (1990) *J. Magn. Reson.*, **88**, 72–85.

Cavanagh, J., Fairbrother, W.J., Palmer III, A.G. and Skelton, N.J. (1996) *Protein NMR Spectroscopy*, Academic Press, New York, NY.

Clubb, R.T. and Wagner, G. (1992) *J. Magn. Reson.*, **97**, 213–217.

Clubb, R.T., Thanabal, V. and Wagner, G. (1992a) *J. Biomol. NMR*, **2**, 203–210.

Clubb, R.T., Thanabal, V. and Wagner, G. (1992b) *J. Biomol. NMR*, **2**, 389–394.

Constantine, K.L., Goldfarb, V., Wittekind, M., Friedrichs, M.S., Anthony, J., Ng, S.C. and Müller, L. (1993) *J. Biomol. NMR*, **3**, 41–54.

DeMarco, A. and Wüthrich, K. (1976) *J. Magn. Reson.*, **24**, 201–204.

Eberstadt, M., Gemmecker, G., Mierke, D.F. and Kessler, H. (1995) *Angew. Chem. Int. Ed. Engl.*, **34**, 1671–1695.

Edison, A.S., Abildgaard, F., Westler, W.M., Mooberry, E.S. and Markley, J. (1994) *Methods Enzymol.*, **239**, 3–79.

Fernández, C., Szyperski, T., Bruyère, T., Ramage, P., Mösinger, E. and Wüthrich, K. (1997) *J. Mol. Biol.*, **266**, 576–593.

Friedrichs, M.S., Müller, L. and Wittekind, M. (1994) *J. Biomol. NMR*, **4**, 703–726.

Gooley, P.R., Johnson, B.A., Marcy, A.I., Cuca, G.C., Salowe, S.P., Hagmann, W.K., Esser, C.K. and Springer, J.P. (1993) *Biochemistry*, **32**, 13098–13108.

Grzesiek, S. and Bax, A. (1992a) *J. Magn. Reson.*, **99**, 201–207.

Grzesiek, S. and Bax, A. (1992b) *J. Am. Chem. Soc.*, **114**, 6291–6293.

Grzesiek, S. and Bax, A. (1993a) *J. Biomol. NMR*, **3**, 185–204.

Grzesiek, S. and Bax, A. (1993b) *J. Am. Chem. Soc.*, **115**, 12593–12594.

Güntert, P., Dötsch, V., Wider, G. and Wüthrich, K. (1992) *J. Biomol. NMR*, **2**, 619–629.

Hardman, C.H., Broadhurst, R.W., Raine, A.R.C., Grasser, K.D., Thomas, J.O. and Laue, E.D. (1995) *Biochemistry*, **34**, 16596–16607.

Ikura, M., Kay, L.E. and Bax, A. (1990) *Biochemistry*, **29**, 4659–4667.

Kay, L.E., Torchia, D.A. and Bax, A. (1989) *Biochemistry*, **28**, 8972–8979.

Kay, L.E., Ikura, M., Tschudin, R. and Bax, A. (1990a) *J. Magn. Reson.*, **89**, 496–514.

Kay, L.E., Ikura, M. and Bax, A. (1990b) *J. Am. Chem. Soc.*, **112**, 888–889.

Kay, L.E., Wittekind, M., McCoy, M.A., Friedrichs, M.S. and Müller, L. (1992) *J. Magn. Reson.*, **98**, 443–450.

Löhr, F. and Rüterjans, H. (1995) *J. Biomol. NMR*, **6**, 189–197.

Luginbühl, P., Szyperski, T. and Wüthrich, K. (1995) *J. Magn. Reson.*, **B109**, 229–233.

Luginbühl, P., Pervushin, K.V., Iwai, H. and Wüthrich, K. (1997) *Biochemistry*, **36**, 7305–7312.

Lukin, J.A., Grove, A.P., Talukdar, S.N. and Ho, C. (1997) *J. Biomol. NMR*, **9**, 151–166.

Marion, D. and Wüthrich, K. (1983) *Biochem. Biophys. Res. Commun.*, **113**, 967–974.

Marion, D., Ikura, K., Tschudin, R. and Bax, A. (1989) *J. Magn. Reson.*, **85**, 393–399.

Matsuo, H., Hanjun, L. and Wagner, G. (1996) *J. Magn. Reson.*, **B110**, 112–115.

Montelione, G.T. and Wagner, G. (1989a) *J. Am. Chem. Soc.*, **111**, 5474–5475.

Montelione, G.T. and Wagner, G. (1989b) *J. Magn. Reson.*, **87**, 183–188.

Morelle, N., Brutscher, B., Simorre, J.-P. and Marion, D. (1995) *J. Biomol. NMR*, **5**, 154–160.

Moy, F.J., Lowry, D.F., Matsumura, P., Dahlquist, F.W., Krywko, J.E. and Domaille, P.J. (1994) *Biochemistry*, **33**, 10731–10742.

Neri, D., Wider, G. and Wüthrich, K. (1992a) *Proc. Natl. Acad. Sci. USA*, **89**, 4397–4401.

Neri, D., Wider, G. and Wüthrich, K. (1992b) *FEBS Lett.*, **303**, 129–135.

Neri, D., Billeter, M. and Wüthrich, K. (1992c) *J. Mol. Biol.*, **223**, 743–767.

Nietlispach, D., Clowes, R.T., Broadhurst, R.W., Ito, Y., Keeler, J., Kelly, M., Ashurst, J., Oschkinat, H., Domaille, P. and Laue, E.D. (1996) *J. Am. Chem. Soc.*, **118**, 407–415.

Nirmala, N.R. and Wagner, G. (1988) *J. Am. Chem. Soc.*, **110**, 7557–7558.

Olejniczak, E.T., Xu, R.X., Petros, A.M. and Fesik, S.W. (1992) *J. Magn. Reson.*, **100**, 444–450.

Otting, G. and Wüthrich, K. (1988) *J. Magn. Reson.*, **76**, 569–574.

Otting, G. and Wüthrich, K. (1990) *Q. Rev. Biophys.*, **23**, 39–96.

Otting, G., Liepinsh, E. and Wüthrich, K. (1991) *Science*, **254**, 974–980.

Palmer III, A.G., Cavanagh, J., Wright, P.E. and Rance, M. (1991) *J. Magn. Reson.*, **93**, 151–170.

Pellecchia, M., Iwai, H., Szyperski, T. and Wüthrich, K. (1997) *J. Magn. Reson.*, **124**, 274–278.
Pellecchia, M., Güntert, P., Glockshuber, R. and Wüthrich, K. (1998) *J. Biomol. NMR*, **11**, 229–230.
Peng, J.W. and Wagner, G. (1992) *J. Magn. Reson.*, **98**, 308–332.
Qian, Y.Q., Otting, G. and Wüthrich, K. (1993) *J. Am. Chem. Soc.*, **115**, 1189–1190.
Rexroth, A., Schmidt, P., Szalma, S., Geppert, T., Schwalbe, H. and Griesinger, C. (1995) *J. Am. Chem. Soc.*, **117**, 10389–10390.
Shaka, A.J., Lee, C.J. and Pines, A.J. (1983) *J. Magn. Reson.*, **52**, 335–338.
Shaka, A.J., Lee, C.J. and Pines, A.J. (1985) *J. Magn. Reson.*, **64**, 547–552.
Shaka, A.J., Lee, C.J. and Pines, A.J. (1988) *J. Magn. Reson.*, **77**, 274–293.
Shan, X., Gardner, K.H., Muhandiram, D.R., Rao, N.S., Arrowsmith, C.H. and Kay, L.E. (1996) *J. Am. Chem. Soc.*, **118**, 6570–6579.
Simorre, J.P., Zimmermann, G.R., Pardi, A., Farmer II, B.T. and Müller, L. (1995) *J. Biomol. NMR*, **6**, 427–432.
Sørensen, O.W., Eich, G.W., Levitt, M.H., Bodenhausen, G. and Ernst, R.R. (1983) *Prog. Nucl. Magn. Reson. Spectrosc.*, **16**, 163–192.
Spera, S. and Bax, A. (1991) *J. Am. Chem. Soc.*, **113**, 5490–5491.
Stephenson, D.S. (1988) *Prog. Nucl. Magn. Reson. Spectrosc.*, **20**, 516–626.
Szyperski, T., Luginbühl, P., Otting, G., Güntert, P. and Wüthrich, K. (1993a) *J. Biomol. NMR*, **3**, 127–132.
Szyperski, T., Wider, G., Bushweller, J.H. and Wüthrich, K. (1993b) *J. Biomol. NMR*, **3**, 151–164.
Szyperski, T., Wider, G., Bushweller, J.H. and Wüthrich, K. (1993c) *J. Am. Chem. Soc.*, **115**, 9307–9308.
Szyperski, T., Pellecchia, M. and Wüthrich, K. (1994a) *J. Magn. Reson.*, **B105**, 188–191.
Szyperski, T., Pellecchia, M., Wall, D., Georgopoulos, C. and Wüthrich, K. (1994b) *Proc. Natl. Acad. Sci. USA*, **91**, 11343–11347.
Szyperski, T., Braun, D., Fernández, C., Bartels, C. and Wüthrich, K. (1995) *J. Magn. Reson.*, **B108**, 197–203.
Szyperski, T., Braun, D., Banecki, B. and Wüthrich, K. (1996) *J. Am. Chem. Soc.*, **118**, 8146–8147.
Szyperski, T., Fernández, C. and Wüthrich, K. (1997) *J. Magn. Reson.*, **128**, 228–232.
Wider, G. and Wüthrich, K. (1993) *J. Magn. Reson.*, **B102**, 239–241.
Wishart, D.S., Sykes, B.D. and Richards, F.M. (1991) *J. Mol. Biol.*, **222**, 311–333.
Wishart, D.S., Bigam, C.G., Yao, J., Abildgaard, F., Dyson, J., Oldfield, E., Markley, J.L. and Sykes, B.D. (1995) *J. Biomol. NMR*, **6**, 135–140.
Wittekind, M. and Müller, L. (1993) *J. Magn. Reson.*, **B101**, 201–205.
Wüthrich, K. (1976) *NMR in Biological Research: Peptides and Proteins*, North Holland, Amsterdam.
Wüthrich, K. (1986) *NMR of Proteins and Nucleic Acids*, Wiley, New York, NY.
Yamazaki, T., Kay, J.D. and Kay, L.E. (1993) *J. Am. Chem. Soc.*, **115**, 11054–11055.
Yamazaki, T., Muhandiram, R. and Kay, L.E. (1994a) *J. Am. Chem. Soc.*, **116**, 8266–8278.
Yamazaki, T., Lee, W., Arrowsmith, C.H., Muhandiram, D.R. and Kay, L.E. (1994b) *J. Am. Chem. Soc.*, **116**, 11655–11666.
Zhang, W., Smithgall, T.E. and Gmeiner, W.H. (1996) *J. Magn. Reson.*, **B111**, 305–309.
Zerbe, O., Szyperski, T., Ottiger, M. and Wüthrich, K. (1996) *J. Biomol. NMR*, **7**, 99–106.
Zimmerman, D.E., Kulikowski, C., Wang, L., Lyons, B. and Montelione, G.T. (1994) *J. Biomol. NMR*, **4**, 241–256.
Zimmerman, D.E. and Montelione, G.T. (1995) *Curr. Opin. Struct. Biol.*, **5**, 664–673.

Appendix

Multidimensional NMR experiments can be compared in terms of resolution, i.e. the precision of the chemical shift measurement, and in terms of dispersion, i.e. the distribution of peaks encoding chemical shifts in one or several dimensions. With regard to the spectral dispersion, it is a novel feature of reduced-dimensionality experiments recorded with simultaneous acquisition of central peaks (Szyperski et al., 1995, 1996) that the loss of dispersion arising from the projection can be recovered by symmetrization about the position of the central peaks, since this eliminates peak doublets with (nearly) degenerate chemical shifts in the other dimensions (Figure 5). The resolution of a NMR experiment depends on the maximal evolution times, t_{max}, and the transverse relaxation times of the observed nuclei. In constant-time evolution periods the transverse relaxation is manifested by signal attenuation and not by line-broadening. Then, t_{max} is the key variable determining the resolution, and the same holds if t_{max} is shorter than the corresponding transverse relaxation time.

Increased values of t_{max} in projected experiments

We shall derive a relation for the relative increase in t_{max} upon projection, given that parent and projected spectrum are accumulated with the same total data size. The chemical shifts of two nuclei A and B are measured in two separate indirect dimensions in the parent experiment, and shall be sampled with i and j complex points, respectively. SW(A), SW(B), t_{max}(A) and t_{max}(B) denote the corresponding sweep widths and maximal evolution times. For simplicity, we assume that delayed acquisition starts at 1/SW, so that

$$t_{max}(A) = \frac{i}{SW(A)} \text{ and } t_{max}(B) = \frac{j}{SW(B)} \qquad (A1)$$

In the projected experiment, A and B shall be observed in a common dimension, and A shall be encoded in the in-phase splitting, while the chemical shift of B is detected in quadrature. Moreover, the chemical shift of A shall be scaled by a factor κ (Szyperski et al., 1993c, 1994). To obtain unambiguous resonance assignments, the apparent carrier position for rf-pulses applied to A must be set at the edge of the spectral range. Hence, the sweep width required for the projected experiment amounts to

$$SW(proj) = SW(B) + 2 \cdot \kappa \cdot SW(A) \qquad (A2)$$

Considering that in the conventional experiment the two dimensions are sampled with i and j complex points, the projected dimension can be sampled with $2 \cdot i \cdot j$ complex points. Hence, the maximal evolution times for A and B after projection, $p_{t_{max}}$, are given by

$$^{p}t_{max}(A) = \frac{2 \cdot \kappa \cdot i \cdot j}{SW(B) + 2 \cdot \kappa \cdot SW(A)} \quad \text{and}$$

$$^{p}t_{max}(B) = \frac{2 \cdot i \cdot j}{SW(B) + 2 \cdot \kappa \cdot SW(A)} \qquad (A2)$$

thus yielding a relative increase in t_{max} which is denoted ϵ(A) and ϵ(B) for A and B, respectively:

$$\epsilon(A) = \frac{^{p}t_{max}(A)}{t_{max}(A)} = \frac{j}{1 + \frac{SW(B)}{2 \cdot \kappa \cdot SW(A)}} \quad \text{and}$$

$$\epsilon(B) = \frac{^{p}t_{max}(B)}{t_{max}(B)} = \frac{i}{\frac{1}{2} + \frac{\kappa \cdot SW(A)}{SW(B)}} \qquad (A4)$$

Given the sweep widths and the data size of the 4D experiment, Equation (A4) allows to calculate the concomitant increase of t_{max} as a function of κ. If the ratio of the maximal evolution times shall be preserved upon projection one has to set $\kappa = t_{max}(A)/t_{max}(B)$, so that Equations (A1) and (A4) yield

$$\epsilon = \epsilon(A) = \epsilon(B) = \frac{2 \cdot i \cdot j}{2 \cdot i + j} \qquad (A5)$$

In this case the relative increase in t_{max} becomes independent of the sweep widths.

Comparison of implementations of 4D spectra with their projected counterpart

Assuming that the maximal evolution time in the direct dimension is equal for projected and parent experiment, the maximal evolution time in the third indirect dimension serving to observe a nucleus C remains to be considered for a comparison of implementations of a 4D experiment and its projected counterpart. We denote the ratios of the maximal evolution times as

$$\theta(A) = \frac{^{4D}t_{max}(A)}{^{p4D}t_{max}(A)}, \; \theta(B) = \frac{^{4D}t_{max}(B)}{^{p4D}t_{max}(B)} \quad \text{and}$$

$$\theta(C) = \frac{^{4D}t_{max}(C)}{^{p4D}t_{max}(C)} \qquad (A6)$$

where the superscript 'p4D' stands for 'projected 4D'. The corresponding average is given by

$$\theta_{av} = \frac{1}{3} \cdot [\theta(A) + \theta(B) + \theta(C)] \qquad (A7)$$

If the indirect dimensions of the 4D experiment are sampled with ${}^{4D}d = i \cdot j \cdot k$ complex points, a 4D spectrum achieving the same maximal evolution times as the projected one would correspond to an extended data matrix comprising ${}^{4Dex}d$ complex points, with

$$ {}^{4Dex}d = \mathrm{int}[i \cdot \theta^{-1}(A)] \cdot \mathrm{int}[j \cdot \theta^{-1}(B)] \cdot \mathrm{int}[k \cdot \theta^{-1}(C)] \quad \text{(A8)} $$

The measurement time of a multidimensional NMR experiment is proportional to its acquired real data size. Setting the sum of the relaxation delay, the time to prepare detectable magnetization and the acquisition time to a commonly used value, i.e., one second, the minimal measurement times (achieved with one scan per real data point) to record the projected 4D, ${}^{p4D}m_{min}$, to record the parent 4D, ${}^{4D}m_{min}$, and to record the parent 4D with extent data size, ${}^{4Dex}m_{min}$, are given (in h) by:

$$ {}^{p4D}m_{min} = \frac{4 \cdot 1 \cdot m}{3600}, \quad {}^{4D}m_{min} = \frac{8 \cdot i \cdot j \cdot k}{3600} \text{ and} $$

$$ {}^{4Dex}m_{min} = \frac{8 \cdot \mathrm{int}[i \cdot \theta^{-1}(A)] \cdot \mathrm{int}[j \cdot \theta^{-1}(B)] \cdot \mathrm{int}[k \cdot \theta^{-1}(C)]}{3600} \quad \text{(A9)} $$

respectively.